Full-field optical coherence tomography-An educational setup for an undergraduate lab

Kai Pieper, Gaël Latour, Jens Küchenmeister, Antje Bergmann, Roman Dengler, Carsten Rockstuhl

Full-field optical coherence tomography—An educational setup for an undergraduate lab

Kai Pieper, Gaël Latour, Jens Küchenmeister, Antje Bergmann, Roman Dengler, and Carsten Rockstuhl

Citation: American Journal of Physics **88**, 1132 (2020); doi: 10.1119/10.0001755
View online: https://doi.org/10.1119/10.0001755
View Table of Contents: https://aapt.scitation.org/toc/ajp/88/12
Published by the American Association of Physics Teachers

Full-field optical coherence tomography—An educational setup for an undergraduate lab

Kai Pieper[a)]
Institute of Theoretical Solid State Physics, Karlsruhe Institute of Technology, Wolfgang-Gaede-Str. 1, 76131 Karlsruhe, Germany and Institute of Physics and Technical Education, Karlsruhe University of Education, 76133 Karlsruhe, Germany

Gaël Latour
Laboratory for Optics and Biosciences, Ecole Polytechnique, CNRS, INSERM, Institut Polytechnique de Paris, Palaiseau, France and UFR Sciences, Université Paris-Saclay, Saint-Aubin, France

Jens Küchenmeister[b)]
Thorlabs GmbH, Münchner Weg 1, 85232 Bergkirchen, Germany

Antje Bergmann [c)]
Institute of Theoretical Solid State Physics, Karlsruhe Institute of Technology, Wolfgang-Gaede-Str. 1, 76131 Karlsruhe, Germany

Roman Dengler
Institute of Physics and Technical Education, Karlsruhe University of Education, 76133 Karlsruhe, Germany

Carsten Rockstuhl
Institute of Theoretical Solid State Physics, Karlsruhe Institute of Technology, Wolfgang-Gaede-Str. 1, 76131 Karlsruhe, Germany and Institute of Nanotechnology, Karlsruhe Institute of Technology, P.O. Box 3640, 76021 Karlsruhe, Germany

(Received 14 August 2019; accepted 21 July 2020)

Optical coherence tomography, or in short OCT, is a measurement technique established in the early 1990s for the non-invasive imaging of interfaces in the bulk of biological tissues or other samples. A full-field OCT setup is built from a microscope combined with a Michelson interferometer, where the mirror in one arm is replaced by the sample. Using white light, which is temporally partially coherent, interference fringes disclose the presence of an interface whenever the lengths of both interferometer arms are nearly equal. Scanning one arm allows for a volumetric reconstruction of all interfaces inside the sample. While the importance of OCT in medicine is indisputable, it is hard to teach students the basic aspects of such technology as most available setups tend to be rather complex. It is our purpose to present a fully functional full-field OCT setup that is stripped-down to its essential components and to promote its use in an undergraduate lab course. The contribution is complemented by a description of the basic theory necessary to understand the working principle of OCT.
https://doi.org/10.1119/10.0001755

I. INTRODUCTION

The idea of using a white light interferometer to gather depth information from samples came up in the 1970s.[1] This idea led to the development of the optical coherence tomography, or in short OCT, in the early 1990s.[2,3] OCT makes it possible to analyse the bulk of tissues and other samples non-invasively[4] by getting a three-dimensional representation of interfaces inside the samples. OCT is nowadays a routine technique that finds applications in medicine, for instance, in Ophthalmology,[5] Cardiology,[6] and Dermatology,[7] and the analysis of artworks.[8,9]

The typical full-field OCT setup comprises a microscope, responsible to provide spatial resolution in the lateral direction, combined with a Michelson interferometer, responsible to provide spatial resolution in the axial direction. At the heart of the OCT is a properly chosen illumination source. It should be a white light source; or at least a source with a finite spectral width that is temporally partially coherent. As we will argue further below, the broader the spectrum is, the better the spatial resolution in the axial direction. Inside the Michelson interferometer, one mirror is replaced by a sample. The sample can be a volumetric one, but it has to comprise interfaces among different materials from where light is partially reflected. Also, the sample should be sufficiently transparent in the spectral region of the source to allow for imaging inside the bulk.

The measurement technique is based on detecting a possible interference among the light reflected from the reference mirror and from the partially reflecting interfaces inside the sample. Because the light is temporally partially coherent, interference fringes emerge in the interferometer only when the path difference of the two arms of the Michelson interferometer is smaller than the effective coherence length. For white light, the reference arm and the sample arm have approximately an equal length. Detecting the spatial locations in the lateral plane where interference occurs allows one to generate volumetric images from the sample where its internal interfaces are mapped out. Nowadays, there exist two large classes of OCT methods.

On the one hand, a frequency-domain OCT detects the reflecting planes by the use of a spectrometer at the output of the Michelson interferometer that divides the light into its component frequencies. Due to the Wiener–Khintchine Theorem, it is possible to reconstruct the position of the

reflecting interfaces of the sample by carrying out a Fourier transform of the detected intensity spectrum.

On the other hand, a time-domain setup detects the interference of the light by moving the sample in the axial direction. The resulting interference patterns are captured by a photodiode (sequential) or a camera (full-field). Detecting an interference contrast in each lateral and axial position provides the desired information about the interfaces in the sample after some image processing. Further information on the various measuring OCT techniques can be found in the literature.[10,11]

Since the early 1990s, OCT has become a very important method for medicine and industry, leading to rapid improvements such as the full-field method[12] and the use of the frequency-domain, allowing one to gather information faster or even to image the whole depth of the sample at once. In modern setups, an axial resolution in the submicron range can be reached.[13–15] The importance of such technology prompts for its consideration in a modern curriculum of undergraduate students.

For this purpose, some approaches for educational or low cost setups were reported.[16–18] However, they mostly concentrate on frequency-domain setups. Although these frequency-domain setups may be more powerful than time-domain setups,[19] they have the disadvantage of being simultaneously much more complex. This complicates the understanding of the basic principles and prompts for an implementation of an OCT that is simultaneously simple and educative while fully preserving its functionality. The concept of coherence, which is the basic concept of OCT, is a very important topic in modern optics lectures. Therefore, many setups exist for educational purposes.[20–23]

This paper is written with the purpose to design an educational full-field OCT setup suitable for undergraduate university or upper high-school students. Its entire design is geared towards making its working principle understandable for students and to demonstrate the functionality by using carefully selected samples in the relevant length scales adapted to the spatial resolution of our instrument.

In Sec. II, we outline the underlying theory necessary to understand the image formation in an OCT setup. Essentially, we have to discuss the emergence of an interference contrast in a Michelson interferometer considering temporally partially coherent light. The text is written with the purpose of being self-contained, and many of the basic aspects are presented in a somewhat condensed manner. In Sec. III, we describe the experimental setup and demonstrate the functionality when discussing a set of carefully selected samples. At the end, we provide some conclusions on our work in a devoted section.

II. THEORY

A. Temporally coherent areas

In order to understand the basic concept of OCT, it is indispensable to start the discussion with the concept of temporal coherence of light. Temporal coherence can best be explained by considering the light emitted from a small source, consisting of a few emitters. This restriction to a small source implies that we consider spatially coherent light. From that source, light is emitted at a central frequency, but the phase of the emitted light experiences irregular discontinuities, so-called phase jumps. These jumps can be explained on phenomenological grounds as being caused by impacts among the emitters. The real part of the emitted electric field is schematically shown in Fig. 1. Within the times t_n between two phase jumps, the wave is perfectly periodic and called temporally coherent. We call these time intervals temporally coherent areas, in analogy to spatially coherent areas.[24,25] The average time between the phase jumps is called the coherence time τ_c.

Frankly speaking, a fixed phase relation exists only for the field within one temporally coherent area, while there is no fixed phase relation for the field among adjacent temporally coherent areas or those further apart in time. This fixed phase relation, however, is important to measure the appearance of interference phenomena as discussed further below.

To mathematically capture the ability of light to cause interference and to describe its temporal coherence, one can rely on the autocorrelation function.[26] The autocorrelation function is given by

$$G(\mathbf{r},\tau) = \lim_{T\to\infty} \frac{1}{2T} \int_{-T}^{T} u^*(\mathbf{r},t)u(\mathbf{r},t+\tau)\mathrm{d}t, \tag{1}$$

with the electric field strength $u(\mathbf{r},t)$ written as a complex analytic signal, described here in the scalar approximation, which is not measurable in experimental setups. It can be said that the autocorrelation function expresses how much information we have on the scalar fields $u(\mathbf{r},t+\tau)$ and $u(\mathbf{r},t)$. With that it serves as a measure to evaluate the average extent of the temporally coherent areas. In the expression above, this is done by comparing the signal $u(\mathbf{r},t)$ with the signal $u(\mathbf{r},t+\tau)$ temporally shifted by τ inside the interval $[-T,T]$. Therefore, we call τ the delay time.

The autocorrelation function also contains information on the intensity

$$I(\mathbf{r}) = \langle |u(\mathbf{r},t)|^2 \rangle = \lim_{T\to\infty} \frac{1}{2T} \int_{-T}^{T} u^*(\mathbf{r},t)u(\mathbf{r},t)\mathrm{d}t \tag{2}$$

of the electric field. To end up with a quantity that does not depend on the intensity and is measurable in experimental setups, the degree coherence

$$|g(\mathbf{r},\tau)| = \left| \frac{G(\mathbf{r},\tau)}{G(\mathbf{r},0)} \right| \tag{3}$$

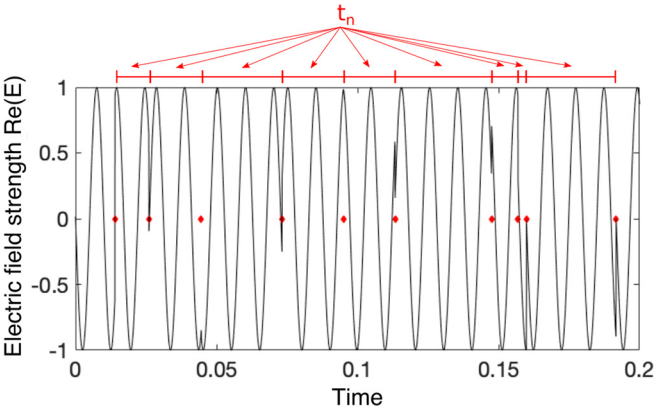

Fig. 1. Schematic illustration of the temporal propagation of an electromagnetic wave (only the electric field) with phase jumps (marked with red points) caused by impacts of the surrounding on the emitting point source.

is introduced, with $G(\mathbf{r},0) = I(\mathbf{r})$. This is just the autocorrelation function normalized to the intensity of the signal. The degree of coherence ranges between zero and unity.

An electric field oscillating at a fixed frequency without discontinuities in the phase would be characterized by a single frequency, by definition. Now, the presence of these phase discontinuities as shown in Fig. 1 automatically implies that more frequency components are required to contribute to the signal. This implies that a partially temporally coherent light source is characterized by a frequency spectrum with a finite spectral width. This will be discussed in detail below, but intuitively it can be estimated that the more abrupt and the more often these jumps occur, the broader the frequency spectrum and vice versa. The degree of coherence for a light source with a Gaussian spectrum is schematically shown in Fig. 2.

The degree of coherence is a measure for the correlation of the phases of the signal $u(\mathbf{r},t)$. The larger the value of $|g(\mathbf{r},\tau)|$ the more likely it is that the phase is correlated when considering the electric field at t and at $t+\tau$.

Even though multiple definitions exist, we consider here the time delay at which the degree of coherence takes the value of $1/2$ as the coherence time τ_c. As mentioned above, it corresponds to the average size of the temporally coherent areas. As already indicated before, the central frequency ω_0 and the spectral width of the spectrum $\Delta\omega$ have great influence on the temporal part of the degree of coherence $g(\tau)$. This relation is mathematically described by the Wiener–Khintchine Theorem.[26] The theorem states that the autocorrelation function $G(\tau)$ and the spectral power density $S(\omega)$ form a Fourier transform pair expressed by

$$G(\tau) = \int_{\infty}^{\infty} S(\omega) e^{-i\omega\tau} d\omega. \tag{4}$$

This means that the degree of temporal coherence $|g(\tau)|$ can be evaluated from the spectral power density $S(\omega)$ and vice versa[27,28] using Eqs. (3) and (4).

Assuming a Gaussian distribution for the degree of temporal coherence and with the help of the Wiener–Khintchine Theorem, the coherence time can be analytically expressed as

$$\tau_c = \frac{1}{\Delta f} = \frac{\lambda_0^2}{c \cdot \Delta\lambda}, \tag{5}$$

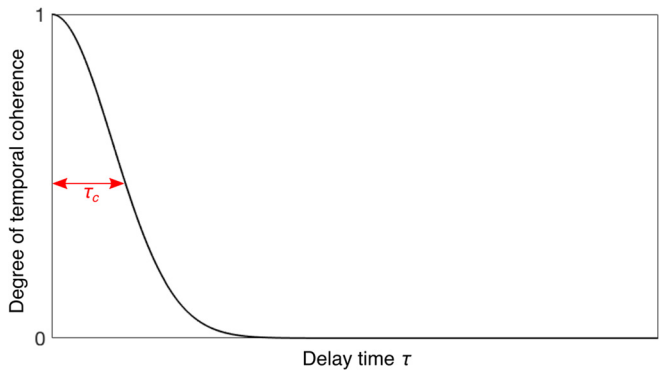

Fig. 2. Schematic representation of the degree of coherence. The average size of the temporally coherent areas corresponds to the half width (marked in red) of the temporal part of the degree of coherence $g(\tau)$, which is defined as the coherence time τ_c.

with the central wavelength λ_0, the spectral width $\Delta\lambda$ of the light source, the frequency uncertainty $\Delta f = \Delta\omega/2\pi$, and c the speed of light.

Now that we have a description for partially temporally coherent light at hand, we can consider the formation of interference patterns in a Michelson interferometer using such a light source.

B. Interference with a Michelson interferometer

The Michelson interferometer, schematically shown in Fig. 3, consists of a light source, two mirrors, a beamsplitter, and a screen. It generates an interference pattern on the screen with an interference contrast depending on the temporal coherence of the illuminating light and the lengths of the two interferometer arms.

We denote $I_1 = \langle |u(\mathbf{r},t)|^2 \rangle$ as the intensity coming from the first arm of the Michelson interferometer and $I_2 = \langle |u(\mathbf{r},t+\tau)|^2 \rangle$ as the intensity coming from the second arm with the respective electric field strength $u(\mathbf{r},t)$ and $u(\mathbf{r},t+\tau)$. The time delay τ that appears in the expression for the intensity in the second arm corresponds to the time difference that elapsed because the light in the second arm might have taken a shorter or a longer path as compared to the first arm. The intensity at the point $\mathbf{r}$ on a screen behind the Michelson interferometer is given by

$$I(\mathbf{r}) = I_1(\mathbf{r}) + I_2(\mathbf{r}) + 2\sqrt{I_1(\mathbf{r}) I_2(\mathbf{r})}\,|g(\mathbf{r},\tau)| \cos\varphi \tag{6}$$

with the phase difference φ depending on the path difference inside the arms of the Michelson interferometer and the degree of coherence $|g(\mathbf{r},\tau)|$ evaluated at the delay time τ. The contrast of such an interference pattern is given by

$$\nu = \frac{I_{\max} - I_{\min}}{I_{\max} + I_{\min}}, \tag{7}$$

where $I_{\max}$ is the intensity of an interference maximum and $I_{\min}$ is the intensity of a neighbouring interference minimum. The extremal values for the intensity are obtained whenever $\cos\varphi = \pm 1$, leading to

$$\nu = 2\frac{\sqrt{I_1 I_2}}{I_1 + I_2}\,|g(\mathbf{r},\tau)|. \tag{8}$$

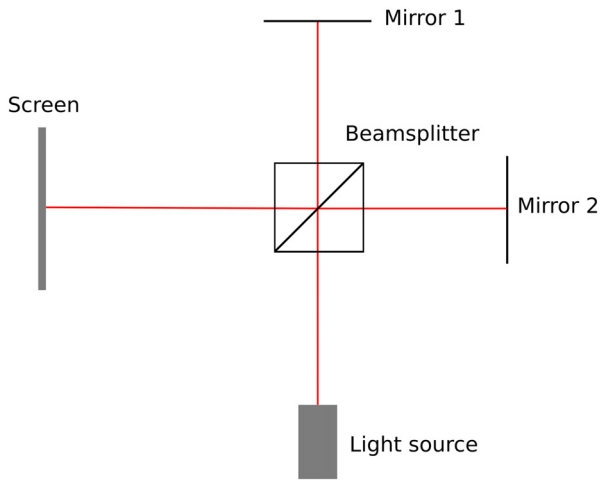

Fig. 3. Sketch of a Michelson interferometer, consisting of a light source, a beamsplitter, two mirrors, and a screen.

From this equation, it can be seen that the contrast within the Michelson interferometer is related to the degree of coherence in relation to the length difference of the two arms in the interferometer. We can conclude that an interference pattern is only visible, defined here as $0 < \nu < 1$, if the coherence time τ_c is longer than the delay time τ. The interference pattern vanishes, defined here as $\nu = 0$, if the delay time τ is much longer than the coherence time τ_c. To observe interference, the temporally coherent areas, therefore, have to be sufficiently "long" to interfere.

The equivalent coherence length corresponds to the difference in the optical path between the two interferometer arms that allows one to see clearly defined interference patterns. By moving one of the mirrors of a Michelson interferometer and capturing the intensity with a photodetector, one can obtain a so-called interferogram, which is shown as a simulation in Fig. 4. It illustrates the sequence of intensity maxima and minima with a specific envelope.

The envelope of the interferogram corresponds to the autocorrelation function of the illuminating light formed by the displacement of the mirrors. So, the envelope of the interferogram corresponds to the degree of temporal coherence. This means that the half width of the interferogram corresponds to the coherence length l_c or, equivalently, to the coherence time τ_c. In Fig. 4, one must keep in mind that the light inside the Michelson interferometer has to pass the displacement of the mirrors twice. An interferogram can be observed, if the moving mirror is within the distances $d_{\text{ref}} \pm l_c/2$ to the beamsplitter, where d_{ref} is the distance of the reference mirror to the beamsplitter. As described in Sec. II A, the width of the interferogram depends on the emitted central wavelength λ_0 and the spectral width $\Delta\lambda$ of the light source. The maximum intensity of the interferogram depends on the intensity of the reflected light. Key to the image formation of a full-field OCT is now the assumption that the mere presence of an interferogram signifies the presence of an interface, if an absolute coordinate system is well-defined.

C. Image formation in a full-field OCT

The actual setup of a simple full-field OCT, as shown in Fig. 5, consists of an interferometric microscope: a combination of a Michelson interferometer and a microscope. This combination is used to detect the interferograms coming

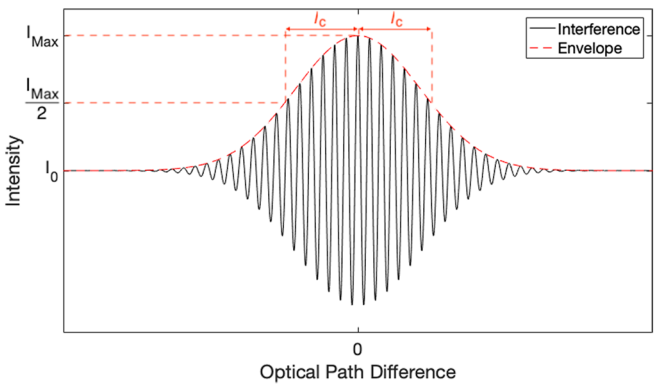

Fig. 4. Simulated interferogram of two light beams interfering inside a Michelson interferometer by Eq. (6). The assumption of a Gaussian shape of the degree of temporal coherence was made. This means that the spectrum of the simulated light-emitting diode (LED) is Gaussian as well.

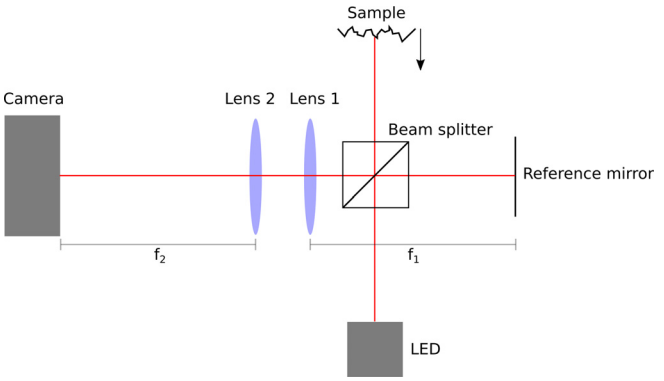

Fig. 5. Schematic illustration of a simple OCT setup.

from the interference of the light in the two arms of the Michelson interferometer.

The Michelson interferometer, consisting of a beam splitter, a reference mirror, and a sample instead of the second mirror, is illuminated by a white light source, for example, a light-emitting diode (LED). The central wavelength λ_0 and the spectral width of the LED $\Delta\lambda$ lead to a rather short coherence time τ_c and, therefore, to a short equivalent coherence length $l_c = c\tau_c$.

The lenses image the surface of the reference mirror and a reference plane of the sample onto the camera chip. The reference plane of the sample is determined by the distance of the reference mirror to the beam splitter. The reference plane and the surface of the reference mirror are inside the focal plane of the first lens. Therefore, the camera chip has to be placed inside the focal plane of the second lens to achieve a sharp image. To scan the sample, the sample is moved axially while the camera is capturing images. In particular, the optical path, the path that the light travels, is twice the moved distance of the sample. This is caused by the geometry of the Michelson interferometer. Another difficulty concerning OCT is that the speed of light c and, therefore, the optical path inside the sample depends on the refractive index n of the material of the sample as well.[29] This means that the exact geometrical position of an interface can only be evaluated if the exact refractive index of the material is known. For the samples we have in mind, the relevant interfaces are not perfectly but only partially reflecting and the refractive index is close to $n_{\text{glass}} = 1.5$. This allows one to have a look inside the samples and to detect a sequence of interfaces.

As said before, the camera detects an interferogram every time a partially reflecting plane of the sample is within the distances $d_{\text{ref}} \pm l_c/2$ relative to the beam splitter, where d_{ref} is the distance of the reference mirror to the beamsplitter. These interferograms contain the depth information of the sample and can be evaluated.

The width of the interferogram is defined by the coherence length, meaning that the axial resolution is related to the coherence length of the light source. Two planes inside the sample can be seen as separated, if the distance between the planes is larger than l_c. The lateral resolution is given by the resolution of the microscope.

III. SETUP AND MEASUREMENTS

Now that we have understood and presented the image formation in the OCT setup, we discuss the experimental aspects of the setup and present selected measurements.

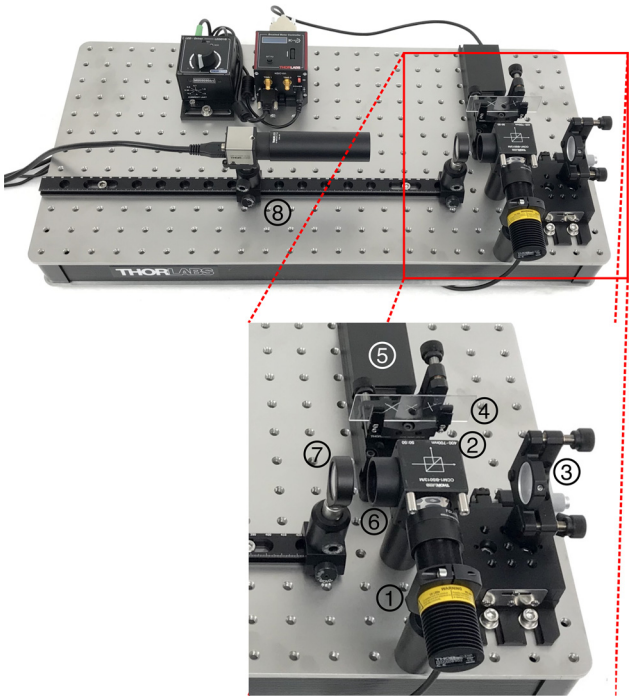

Fig. 6. Full-field time-domain OCT setup, according to the illustration in Fig. 5, consisting of an LED 1, a beam splitter 2, the reference mirror blank 3, the sample on a motorized stage 4 + 5, two lenses 6 + 7, and a camera 8.

A. Components

In this subsection, we will give a short description of the setup and its functionality. The OCT setup, according to the illustration in Fig. 5, is shown in Fig. 6. The used components can be found in Table I.

Basically, the setup consists of two main parts. The first part is the Michelson interferometer, consisting of the beam splitter ②, the reference mirror ③, and the sample ④ with a motorized stage ⑤.

The second part is the microscope, consisting of the lenses ⑥ + ⑦ and the camera chip ⑧. The lenses image the sample and the reference mirror onto the camera chip. Therefore, the sample and the reference mirror are inside the focal plane of lens ⑥, while the camera chip is in the focal plane of lens ⑦. We have a magnification of $M = 200\,\text{mm}/75\,\text{mm} = 2.66$. The magnification can easily be changed by changing lens ⑦ in front of the camera and repositioning the camera. With the specifications of the camera chip (horizontal extent 6.78 mm with 1280 pixels), we reach a theoretical lateral resolution of $2\,\mu\text{m}/\text{pixel}$ based on the pixel size.

The light used for this setup is generated by a warm white LED with $\lambda_0 = 600\,\text{nm}$, inspired by other setups[30,31] using thermal light in an OCT setup, with a spectral filter ① cutting off the wavelengths below 495 nm in order to receive a nearly Gaussian spectrum with $\Delta\lambda = 125\,\text{nm}$ full width at half maximum. The interferogram of the used LED is shown in Fig. 7. As we can see, the envelope of the interferogram does not exhibit a Gaussian shape since the LED spectrum does not show a perfectly Gaussian distribution. Such an LED offers an equivalent coherence length of $l_c = \tau_c c \approx 2.9\,\mu\text{m}$. This means that we can see interference fringes on the camera each time a reflecting plane of the sample is within the distances $d_{\text{ref}} \pm (2.9/2)\,\mu\text{m}$ to the beam splitter, where d_{ref} is the distance between the beam splitter and the surface of the reference mirror blank. We can see two planes of the sample separated if the distance between these planes is larger than $l_c = 2.9\,\mu\text{m}$. This implies that the axial resolution of the setup is about $2.9\,\mu\text{m}$.

Table I. List of components used to build the OCT setup.

① LED with filter	Thorlabs MWWHL4 and Thorlabs FGL495M
② Beam splitter	Thorlabs CCM1-BS013/M
③ Reference mirror	Thorlabs PF10-03
④ Sample	Scratch in a glass slide
⑤ Motorized stage	Thorlabs MTS25/M-Z8
⑥ Lens 75 mm	Thorlabs AC254-75-A
⑦ Lens 200 mm	Thorlabs AC254-200-A
⑧ Camera	Thorlabs DCC3240M

B. Alignment

The alignment of the setup is very easy. One would start by setting up the Michelson interferometer with a microscope slide instead of a sample, followed by the adjustment of the camera and the lens so that a sharp image of a distant object is visible. For finding the white light interference, one would add the lens ⑥ behind the beam splitter and adjust the distance of the mirror blank to the beam splitter so that a sharp image of the surface of the mirror blank is visible. Afterwards, the microscope slide is moved until a sharp image of its surface is visible. In most cases, the white light interference is already visible at this point. If not, the microscope slide has to be moved further. Finally, the tilting angle of the microscope slide should be adjusted to align it to the mirror blank such that one interference stripe is larger than the field of view.

C. Data and image acquisition

To measure a surface or the interior of a sample, we have to record the interferograms of the sample. Therefore, we move the sample axially and capture images with the camera. We move the stage continuously at $2\,\mu\text{m}/\text{s}$ and take images with the camera at 26.6 frames per second (FPS) continuously. In consequence, the camera takes an image every $\Delta z = 2\,\mu\text{m}/\text{s}/26.6\,\text{FPS} = 75\,\text{nm}$ of stage travel. This is

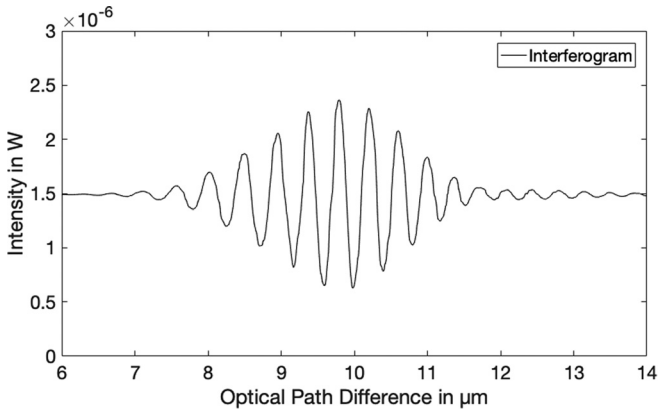

Fig. 7. Interferogram of the used light source with $\lambda_0 = 600\,\text{nm}$ and $\Delta\lambda = 125\,\text{nm}$. Each signal from the sample is convoluted with this interferogram. This means that each reflecting surface will have at least the width of this interferogram. Therefore, understanding the relation between the LED spectrum and the interferogram is crucial for understanding the OCT signal.

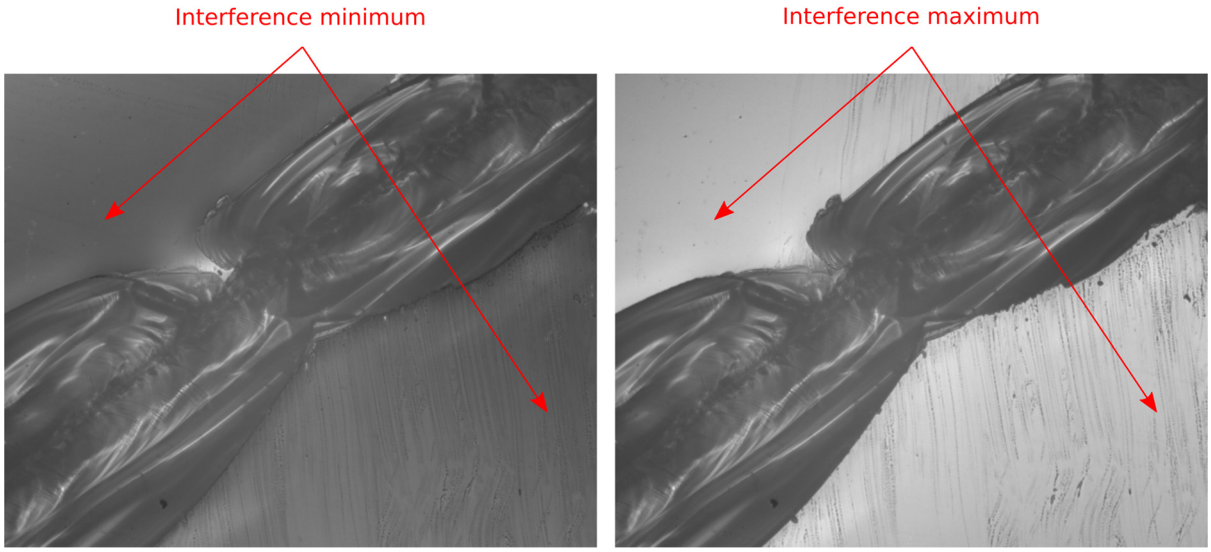

Fig. 8. Interference of the light coming from the sample (scratch in a glass slide) and the reference mirror with stage travel of $\Delta z = 150\,\text{nm}$ between the images.

equivalent to 150 nm in the optical path, because the light has to pass the arm twice in the Michelson interferometer. If a reflecting plane of the sample and the reference mirror have nearly an identical distance to the beam splitter, the images are characterized by brighter or darker areas changing from image to image. These areas are interference fringes of the Michelson interferometer forming interferograms in the axial direction, which will later give the depth information of the sample. Since the interferograms are characterized by a sequence of intensity maxima and minima, a three-dimensional representation of the scanned sample would contain bright and dark stripes in the axial direction. To avoid these stripes and gather a clean position information of the interfaces out of the interferograms, it is necessary to approximate the envelope of the interferograms. To extract the position information and approximate the envelope of the interferograms, we take four consecutive images S_1 to S_4 and evaluate the tomographic image S_T[31]

$$S_T = \frac{1}{2}(|S_1 - S_3| + |S_2 - S_4|). \tag{9}$$

Fig. 9. Tomographic image S_T evaluated in Eq. (9) and four consecutive images S_1–S_4 with 75 nm stage travel in between.

The four images are characterized by grayscale values in unsigned eight-bit integers, with a distance of $\Delta z = 75\,\text{nm}$ of stage travel in between. So, the images S_1 and S_3, like S_2 and S_4, have a distance of $\Delta z = 150\,\text{nm}$ stage travel in between. Because of the central wavelength of our light source, which is about $\lambda_0 = 600\,\text{nm}$, the interference maxima become minima and vice versa every 300 nm in the optical path in air $n_{\text{air}} = 1$, equivalent to 150 nm of stage travel, as shown in Fig. 8 with a sample consisting of a scratch in a glass slide.

Before evaluating the difference images $S_1 - S_3$ and $S_2 - S_4$, the images must be converted to double format to accept negative values. Furthermore, a 2D median filter, smoothing the background noise caused by the gain of the camera chip and the intensity fluctuations of the LED, is applied to the images S_1–S_4.

The resulting tomographic image S_T is shown in Fig. 9. A bright area represents a spot on the sample where light was reflected and interfered with the light inside the reference arm. The areas left and right of the scratch are white, meaning that the plane under investigation is the surface plane of the glass slide. Even though the individual camera images in Fig. 8 show light coming from within the scratch, the tomographic image in Fig. 9 shows a black shape. The reason is that the scratch is too deep: Due to the short coherence length of the light source, the glass slide surface and the

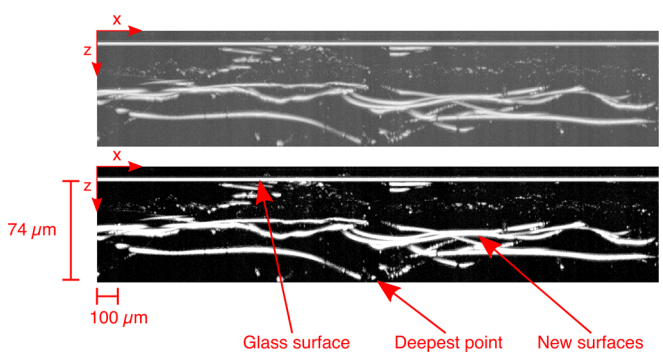

Fig. 10. Evaluation of the data for a scratch in a glass slide in the xz-section. Logarithmic plot (top and bottom) with a threshold right above the background noise (bottom).

bottom of the scratch cannot both show interference with the reference arm at the same time. Therefore, no interference occurs for the light coming from within the scratch and the images S_1–S_4 cancel to zero in Eq. (9) for this region. Naturally, this changes when the stage is moved in the right direction. These are the tomographic images containing an approximation to the envelope of the interferograms in the axial direction. The described evaluation is done by a short Matlab script. With imageJ,[32] it is possible to get a 3D view of all evaluated tomographic images. One can obtain a look on the scratch in the y-direction as shown in Fig. 10 by stacking all of the xz-sections. Here, the xy-plane is a lateral image captured by the camera and z labels the axial direction. We use a logarithmic plot (top and bottom) and reduce the background noise by setting a threshold right above the background noise value (bottom). The representation shows that the glass of the sample containing the scratch is splintered and has formed new surfaces. One can see the glass surface of the microscope slide, in which the scratch was made. Furthermore, it is possible to extract the real depth of the scratch from the data, by counting the images with stage travel of 150 nm in between from the surface to the deepest point. The stage travel for this scan is about 74 μm and corresponds to the real depth of the scratch. This is possible because our representation shows only the glass surfaces, the medium in which the light is propagating is air with refractive index $n_{\text{air}} = 1$. The depth is measured from the surface of the glass slide to the deepest point of the scratch.

D. Samples

The following sample consists of a layer of adhesive tape, as shown in Fig. 11. One can see the layer of plastic, having some inclusions, and the layer of glue. The intensity of the layer of glue decreases because of the high amount of reflected light from the beginning of the plastic layer. This can be compensated by using a logarithmic plot (top and bottom). By setting a threshold right above the background noise, it is possible to filter the data (bottom). The stage travel for this scan is about 78 μm, but we cannot say how thick the layers are, because we do not know the exact refractive index n of the plastic and the glue.

Figure 12 shows the cross section of an ID-card, consisting of multiple layers of plastic and embedded volumetric holograms as security prints. As in the previous sample, we are using a logarithmic plot (top and bottom) and set a threshold right above the background noise to clarify the

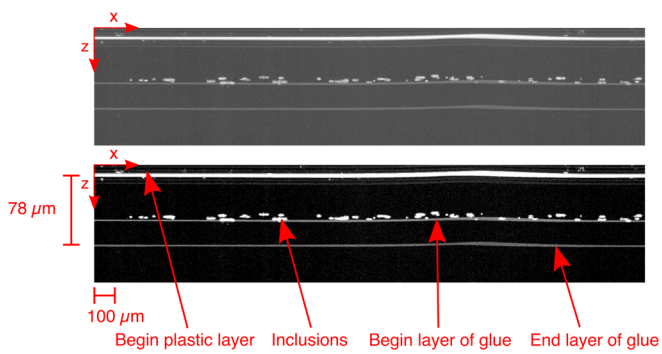

Fig. 11. Evaluation of the data for a layer of adhesive tape on a glass slide. Logarithmic plot (top and bottom) with a threshold right above the background noise (bottom).

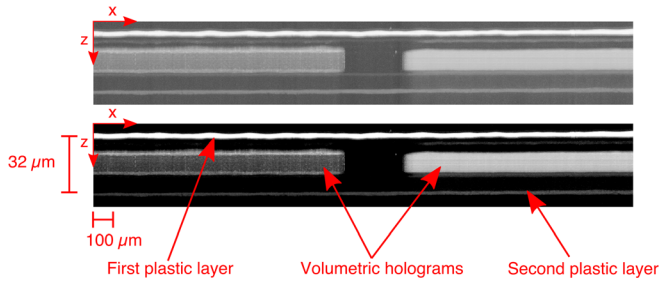

Fig. 12. Evaluation of the data for an ID-card. Logarithmic plot (top and bottom) with a threshold right above the background noise (bottom).

data (bottom). One can see two reflecting planes and two volumetric holograms in between. The reflecting planes are plastic layers of the ID-card, in which the volumetric holograms are embedded. We can also see that the reflected intensities of the holograms are different. This is caused by the different viewing angles of the holograms, when one is looking at the ID-card. The stage travel for this scan is about 32 μm. As with the previous sample, we cannot say how thick the volumetric holograms are, because we do not know the exact refractive index n of the plastic of the ID-card.

IV. CONCLUSION

We have presented what we consider to be a very simple setup for performing full-field optical coherence tomography that is reduced to its basic parts. Despite the simplifications of our OCT setup, it offers a high quality of measurements. Additionally, the alignment of the setup is very simple, meaning that in contrast to research grade setups there are no microscope objectives inside the arms of the Michelson interferometer that have to be aligned properly. Finding the white light interference with the help of the sharp image of the surfaces of the sample and the reference mirror blank is very easy as well. Students can now focus on the basics of OCT and temporal coherence by using this simple and clear setup.

ACKNOWLEDGMENTS

The authors would like to thank Thorlabs GmbH and the joint research project MINT^{2}KA for supporting this project.

[a]Electronic mail: kai.pieper@kit.edu
[b]Electronic mail: JKuechenmeister@thorlabs.com
[c]Electronic mail: antje.bergmann@kit.edu

[1]P. A. Flournoy, R. W. McClure, and G. Wyntjes, "White-light interferometric thickness gauge," Appl. Opt. **11**(9), 1907–1915 (1972).
[2]D. Huang, E. A. Swanson, C. P. Lin, J. S. Schuman, W. G. Stinson, W. Chang, M. R. Hee, T. Flotte, K. Gregory, C. A. Puliafito, et al. "Optical coherence tomography," Science **254**(5035), 1178–1181 (1991).
[3]Thomas Dresel, Gerd Häusler, and Holger Venzke, "Three-dimensional sensing of rough surfaces by coherence radar," Appl. Opt. **31**(7), 919–925 (1992).
[4]D. Stifter, "Beyond biomedicine: A review of alternative applications and developments for optical coherence tomography," Appl. Phys. B **88**(3), 337–357 (2007).
[5]Carmen A. Puliafito, Michael R. Hee, Charles P. Lin, Elias Reichel, Joel S. Schuman, Jay S. Duker, Joseph A. Izatt, Eric A. Swanson, and James G. Fujimoto, "Imaging of macular diseases with optical coherence tomography," Ophthalmology **102**(2), 217–229 (1995).
[6]Ik-Kyung Jang, Brett E. Bouma, Dong-Heon Kang, Seung-Jung Park, Seong-Wook Park, Ki-Bae Seung, Kyu-Bo Choi, Milen Shishkov, Kelly Schlendorf, Eugene Pomerantsev, Stuart L. Houser, H. Thomas Aretz, and Guillermo J. Tearney, "Visualization of coronary atherosclerotic plaques in patients using optical coherence tomography: Comparison with intravascular ultra-sound," J. Am. Coll. Cardiol. **39**(4), 604–609 (2002).

[7]Julia Welzel, "Optical coherence tomography in dermatology: A review," Skin Res. Technol. **7**(1), 1–9 (2001).
[8]Gaël Latour, Jean-Philippe Echard, Balthazar Soulier, and Isabelle Emond, "'Stéphane Vaiedelich and Mady Elias,' Structural and optical properties of wood and wood finishes studied us- ing optical coherence tomography: Application to an 18th century Italian violin," Appl. Opt. **48**(33), 6485–6491 (2009).
[9]Gaël Latour, Julien Moreau, Mady Elias, and Jean-Marc Frigerio, "Micro-spectrometry in the visible range with full-field optical coherence tomography for single absorbing layers," Opt. Commun. **283**(23), 4810–4815 (2010).
[10]P. H. Tomlins and R. K. Wang, "Theory, developments and applications of optical coherence tomography," J. Phys. D: Appl. Phys. **38**(15), 2519–2535 (2005).
[11]Arnaud Dubois, *Handbook of Full-Field Optical Coherence Microscopy - Technology and Applications* (Pan Stanford Publishing Pte. Ltd., Singapore, 2016).
[12]E. Beaurepaire, A. C. Boccara, M. Lebec, L. Blanchot, and H. Saint-Jalmes, "Full-field optical coherence microscopy," Opt. Lett. **23**(4), 244–246 (1998).
[13]B. Povazay, K. Bizheva, A. Unterhuber, B. Hermann, H. Sattmann, A. F. Fercher, W. Drexler, A. Apolonski, W. J. Wadsworth, J. C. Knight, P. St. J. Russell, M. Vetterlein, and E. Scherzer, "Submicrometer axial resolution optical coherence tomography," Opt. Lett. **27**(20), 1800–1802 (2002).
[14]Arnaud Dubois, Laurent Vabre, Albert-Claude Boccara, and Emmanuel Beaurepaire, "High-resolution full-field optical coherence tomography with a linnik microscope," Appl. Opt. **41**(4), 805–812 (2002).
[15]Arnaud Dubois, Kate Grieve, Gael Moneron, Romain Lecaque, Laurent Vabre, and Claude Boccara, "Ultrahigh-resolution full-field optical coherence tomography," Appl. Opt. **43**(14), 2874–2883 (2004).
[16]Joshua Barr, Paul V. Jansz, Steven Hinckley, and Graham Wild, *Low-Cost Educational Optical Coherence Tomography System for Thickness Measurements Tomography System for Thickness Measurements* (ECU Publications, Joondalup, Australia, 2012).
[17]Paritosh Pande, Ryan L. Shelton, Guillermo L. Monroy, Ryan M. Nolan, and Stephen A. Boppart, "Low-cost hand-held probe for depth-resolved low-coherence interferometry," Biomed. Opt. Express **8**(1), 338–348 (2017).
[18]Sanghoon Kim, Michael Crose, Will J. Eldridge, Brian Cox, William J. Brown, and Adam Wax, "Design and implementation of a low-cost, portable OCT system," Biomed. Opt. Express **9**(3), 1232–1243 (2018).
[19]R. Leitgeb, C. K. Hitzenberger, and A. F. Fercher, "Performance of Fourier domain vs. time domain optical coherence tomography," Opt. Express **11**(8), 889–894 (2003).
[20]K. Pieper, A. Bergmann, R. Dengler, and C. Rockstuhl, "Visualizing and manipulating the spatial and temporal coherence of light with an adjustable light source in an undergraduate experiment," Eur. J. Phys. **40**(5), 055302 (2019).
[21]Lorenzo Basano, Carlo Pontiggia, and Emanuele Piano, "Simple demonstrations for introducing spatial coherence," Am. J. Phys. **64**(10), 1257–1261 (1996).
[22]D. Bloor, "Coherence and correlation - Two advanced experiments in optics," Am. J. Phys. **32**(12), 936–941 (1964).
[23]C. R. Wheeler, R. D. Ramsier, and P. N. Henriksen, "An investigation of the temporal coherence length of light," Eur. J. Phys. **24**(4), 443–450 (2003).
[24]K. Pieper, A. Bergmann, R. Dengler, and C. Rockstuhl, "Using a pseudo-thermal light source to teach spatial coherence," Eur. J. Phys. **39**(4), 045303 (2018).
[25]W. Martienssen and E. Spiller, "Coherence and fluctuations in light beams," Am. J. Phys. **32**(12), 919–926 (1964).
[26]Max Born, Emil Wolf, A. B. Bhatia, P. C. Clemmow, D. Gabor, A. R. Stokes, A. M. Taylor, P. A. Wayman, and W. L. Wilcock, *Principles of Optics: Electromagnetic Theory of Propagation, Interference and Diffraction of Light*, 7th ed. (Cambridge U. P., Cambridge, 1999).
[27]Peter J. Millet, "An undergraduate optics experiment on coherence length and bandwidth," Am. J. Phys. **39**(2), 163–166 (1971).
[28]J. C. Albergotti, "Fourier transform spectroscopy using a Michelson interferometer," Am. J. Phys. **40**(8), 1070–1078 (1972).
[29]J. J. Fendley, "Measurement of refractive index using a michelson interferometer," Phys. Educ. **17**(5), 209–211 (1982).
[30]Blandine Laude, Antonello De Martino, Bernard Drévillon, Laurence Benattar, and Laurent Schwartz, "Full-field optical coherence tomography with thermal light," Appl. Opt. **41**(31), 6637–6645 (2002).
[31]Antonello De Martino, David Carrara, Bernard Drévillon, and Laurent Schwartz, "Full-field OCT with thermal light," Proc. SPIE **4431**, 44314431 (2001).
[32]Imagej, <https://imagej.nih.gov>. Accessed on March 21, 2019.